Published in final edited form as:
Stem Cells. 2011 September ; 29(9): 1349–1361. doi:10.1002/stem.684.

Radical Acceleration of Nuclear Reprogramming by Chromatin Remodeling with the Transactivation Domain of MyoD

Hiroyuki Hirai[a,b], **Tetsuya Tani**[a,b,c], **Nobuko Katoku-Kikyo**[a,d], **Steven Kellner**[a,b], **Peter Karian**[a,b], **Meri Firpo**[a,d], and **Nobuaki Kikyo**[a,b]

[a]Stem Cell Institute, University of Minnesota, Minneapolis, Minnesota, USA

[b]Division of Haematology, Oncology and Transplantation, University of Minnesota, Minneapolis, Minnesota, USA

[c]Laboratory of Animal Reproduction, Department of Agriculture, Kinki University, Nara, Japan

[d]Division of Endocrinology, Department of Medicine, University of Minnesota, Minneapolis, Minnesota, USA

Abstract

Induced pluripotent stem cells (iPSCs) can be created by reprogramming differentiated cells through introduction of defined genes, most commonly *Oct4*, *Sox2*, *Klf4*, and *c-Myc* (OSKM). However, this process is slow and extremely inefficient. Here, we demonstrate radical acceleration of iPSC creation with a fusion gene between *Oct4* and the powerful transactivation domain (TAD) of *MyoD* (M_3O). Transduction of M_3O as well as *Sox2*, *Klf4*, and *c-Myc* into fibroblasts effectively remodeled patterns of DNA methylation, chromatin accessibility, histone modifications, and protein binding at pluripotency genes, raising the efficiency of making mouse and human iPSCs more than 50-fold in comparison to OSKM. These results identified that one of the most critical barriers to iPSC creation is poor chromatin accessibility and protein recruitment to pluripotency genes. The MyoD TAD has a capability of overcoming this problem. Our approach of fusing TADs to unrelated transcription factors has far-reaching implications as a powerful tool for transcriptional reprogramming beyond application to iPSC technology.

Keywords

Embryonic stem cells; Induced pluripotent stem cells; MyoD; Oct4

Introduction

Creation of induced pluripotent stem cells (iPSCs) can be achieved through a surprisingly simple approach to nuclear reprogramming [1]. In the original protocol, Takahashi and Yamanaka transduced retrovirus encoding *Oct4*, *Sox2*, *Klf4*, and *c-Myc* (OSKM) into

Correspondence: Nobuaki Kikyo, M.D., Ph.D., Stem Cell Institute, University of Minnesota, MTRF, Room 2-216, 2001 6th St SE, Minneapolis, Minnesota 55455, USA. Telephone: 612-624-0498; Fax: 612-624-2436; kikyo001@umn.edu.

Disclosure of Potential Conflicts of Interest

The authors indicate no potential conflicts of interest.

Author contributions: H.H. and N.K.: conception and design, collection and assembly of data, data analysis and interpretation, manuscript writing, final approval of manuscript; T.T.: conception and design, collection and assembly of data, data analysis and, interpretation, final approval of manuscript; N.K.-K., S.K., and P.K.: collection and assembly of data, final approval of manuscript; M.F.: financial support, data analysis and interpretation, final approval of manuscript.

mouse embryonic fibroblasts (MEFs) and obtained pluripotent cell colonies resembling embryonic stem cells (ESCs) in approximately 2 weeks [2]. However, iPSC protocols are generally very inefficient, with only around 0.1% of MEFs transduced with OSKM forming iPSCs. Although the reasons for this inefficiency are unclear, it is unlikely that gene delivery is responsible given the high efficiency of retrovirus transduction (>90%). Chemicals that relax chromatin, such as inhibitors of histone deacetylation and DNA methylation, can increase the efficiency of iPSC creation [3, 4], suggesting that chromatin structure in host cells may limit nuclear reprogramming through poorly understood epigenetic mechanisms.

Oct4, Sox2, and Nanog constitute a central triad in the molecular circuitry underlying the maintenance of the undifferentiated state and pluripotency of ESCs [5, 6]. These three transcription factors activate their own genes and other pluripotency genes, in addition to suppressing aberrant expression of lineage-specific genes. The *Oct4* gene contains binding sites for the Oct4 and Sox2 proteins in its distal enhancer region [6]. However, transduction of the *Oct4* gene alone or in combination with *Sox2* and *Nanog* can not effectively activate *Oct4* gene expression.

In contrast to Oct4, MyoD, a master transcription factor for skeletal myogenesis, can activate many of its target genes in nonmuscle cells, including its own gene and other skeletal muscle-specific genes, without the aid of additional exogenous factors [7–10]. Because of this potent transcriptional activation (transactivation), MyoD can directly convert one cell type into another, as exemplified by the creation of myotubes from pigmented retinal epithelial cells approximately 10 days after transduction of the *MyoD* gene [11]. These findings suggest that MyoD can recruit various transcription factors and chromatin remodeling proteins to its target genes more efficiently than Oct4, leading to activation of suppressed genes embedded in closed chromatin. Therefore, we hypothesized that fusion of a MyoD fragment to full-length Oct4 might confer upon Oct4, the powerful transactivation capacity of MyoD, without losing the target specificity of Oct4. Through testing this hypothesis, we established a novel approach for dramatically increasing chromatin accessibility and recruitment of chromatin remodeling proteins to the *Oct4* site, resulting in radical acceleration of iPSC generation.

Materials and Methods

Preparation of Mouse iPSCs

Full-length and deletion mutants of mouse *Oct4* cDNA were fused with various transactivation domains (TADs) and inserted into the pMXs-IP vector [12]. Details of the subcloning procedures for each construct are available upon request. Polycistronic cDNAs encoding *Sox2*, *Klf4*, and *c-Myc* were transferred from the 4F2A lentiviral vector [13] to the pMXs-IP vector. pMXs-IP vectors encoding OSKM separately (Addgene, Cambridge, MA, www.addgene.org) were also used in some experiments. These pMXs-IP vectors were transfected into Plat-E cells [14] with Fugene six (Roche, Penzberg, Germany, www.roche-applied-science.com). Virus supernatant was harvested 48- and 72-hour later and filtered through a 0.45-μm syringe filter. MEFs were prepared from Oct4-green fluorescence protein (GFP) mice which harbor an internal ribosome entry site–GFP fusion cassette downstream of the stop codon of the *Oct4* gene (Jackson Laboratory [Bar Harbor, ME, www.jax.org] #008214) [15]. All animal experiments were conducted in accordance with the animal experiment guidelines of University of Minnesota. For chimera experiments, MEFs were prepared from mice that harbor the Oct4-GFP allele and ROSA26-*lacZ* allele. MEFs were seeded at 3×10^5 cells per 6-cm-dish on day −2 in Dulbecco's modified Eagle's medium (DMEM) with 10% fetal bovine serum (FBS). Fresh virus supernatant was added to MEFs on days −1 and 0 with 10 μg/ml polybrene. Culture medium was then changed to iPSC medium (DMEM, 15% FBS, 100 μM minimum essential medium [MEM]

nonessential amino acids, 55 μM 2-mercaptoethanol, 2 mM L-glutamine, and 1,000 u/ml leukemia inhibitory factor) on day 1. Transduced MEFs were subcultured onto irradiated SNL feeder cells at 2×10^5cells per 6 cm dish on day 4 and maintained on the feeder cells in protocol A. The maximum number of GFP-positive colonies obtained around day 18 was divided by 2×10^5 to obtain the efficiency of making iPSCs. In protocol B, transduced MEFs were maintained without feeder cells. GFP-positive colonies were picked up around day 10 to clone without feeder cells for pluripotency analyses. Retrovirus titer was measured using NIH3T3 cells as described [2]. All recombinant DNA research was conducted following the NIH guidelines

Preparation of Human iPSCs

Full-length human *OCT4* cDNA fused with the M_3 domain of human *MYOD* at the amino terminus was inserted into the pMXs-IP vector. pMXs-IP vectors encoding human M_3O and OSKM (Addgene) were transfected into Plat-A cells (Cell Biolabs, San Diego, CA, www.cellbiolabs.com) with Lipofectamin 2000 (Invitrogen, Carlsbad, CA, www.invitrogen.com). Virus supernatant was harvested 48 and 72 hours later (days −1 and 0, respectively, below), filtered through a 0.45-μm syringe filter, and transduced into dermal fibroblasts obtained from a 34-year-old Caucasian female (Cell Applications, San Diego, CA, www.cellapplications.com). On day −2, 2.7×10^4 fibroblasts were plated in each well of a 12-well plate in DMEM with 10% FBS. Fresh virus supernatant was added to the fibroblasts on days −1 and 0 with 10 μg/ml polybrene. On day 3, cells were harvested with trypsin and subcultured at 1.7×10^4 cells per well in 12-well plates coated with BD Matrigel hESC-qualified Matrix (BD Biosciences, San Jose, CA, www.bdbiosciences.com) in human iPSC medium (KnockOut DMEM/F-12 [Invitrogen], 20% Knockout Serum Replacement [Invitrogen], 100 μM MEM nonessential amino acids, 1% insulin-transferrin-selenium [Invitrogen], 0.1 mM 2-mercaptoethanol, 2 mM L-glutamine, and 4 ng/ml basic FGF). The medium was changed every other day.

Chromatin Accessibility to NsiI

One million cells were resuspended in ice-cold lysis buffer containing 0.1% NP40 and incubated on ice for 5 minutes as described previously [16]. Nuclei were isolated with centrifugation at 4,000*g* for 5 minutes and digested with 200 u/ml NsiI for 2 hours at 37°C. DNA was purified and double-digested with MspI and BamHI, followed by Southern blotting using the radioactive probe shown in Figure 5D.

Additional methods are described in Supporting Information Materials and Methods section.

Results

Generation of Mouse iPSCs with Heterologous TADs

We tested our above-mentioned hypothesis with a series of chimeric proteins, in which full-length mouse Oct4 was fused with various fragments of mouse MyoD (Fig. 1A). The basic helix-loop-helix domain of MyoD, important for dimerization and DNA binding, was not included in these constructs to avoid activation of MyoD-target genes. Each chimeric gene was cotransduced with a polycistronic retroviral vector encoding mouse *Sox2*, *Klf4*, and *c-Myc* (SKM) [13] into MEFs derived from Oct4-GFP mice, which contain the GFP gene knocked into the *Oct4* locus [15]. In this model, formation of GFP-positive colonies indicates that individual MEFs develop into Oct4-expressing cells capable of clonal growth. Expression of chimeric proteins was confirmed through immunoblotting with antibodies against Oct4 (Supporting Information Fig. S1). As a control, we transduced MEFs with OSKM (O-MEFs) on days −1 and 0 and transferred these cells onto SNL feeder cells on day 4 following a standard protocol (Fig. 1B, protocol A). GFP-positive colonies emerged

around day 10, gradually increasing in number until reaching a peak by day 18. To calculate the percentage of MEFs that were reprogrammed into iPSCs, we divided the number of GFP-positive colonies by the total number of MEFs seeded in a culture dish. We estimated that 0.08% ± 0.09% of O-MEFs were converted into GFP-positive cells, which is similar to previous reports [2, 3] (Fig. 1A, right column). We then transduced MEFs with each chimeric gene along with SKM and followed the protocol described above (protocol A). M_3O with SKM (M_3O-SKM) increased the percentage of GFP-positive colonies most drastically, with 5.10% ± 0.85% of MEFs (M_3O-MEFs) being transformed into GFP-positive cells by day 15. The M_3 region encompasses the acidic TAD of MyoD (amino acids 3–56) [17], and acidity is considered important to its transactivation capability. However, the simple presence of acidity was insufficient to facilitate iPSC formation, as evidenced by a lack of increase in GFP-positive colonies in MEFs transduced with M_6O, which also contains the main acidic amino acid cluster, or a chain of 20 glutamic acids attached to Oct4 (EO) (Fig. 1A). The high efficiency with which M_3O created iPSCs when compared with Oct4 was not simply due to a difference in the retrovirus titer for the two virus suspensions. The titer for the M_3O virus and Oct4 virus was $1.8 \pm 0.2 \times 10^7$ and $2.1 \pm 0.4 \times 10^7$ colony forming units per milliliter, respectively.

While conducting the above experiments, we noticed that GFP-positive colonies emerged from M_3O-MEFs on approximately day 5 without transfer onto feeder cells (Fig. 1B, protocol B), and these colonies steadily increased in size and number (Fig. 1C). By approximately day 12, 3.6% ± 0.5% of M_3O-MEFs formed GFP-positive colonies in the absence of feeder cells, probably supported by the surrounding MEFs serving as “autologous” feeder cells (Fig. 1D). In contrast, GFP-positive colonies emerged from O-MEFs between days 16 and 18 at an extremely low efficiency (0.0035% ± 0.0006%) with the same protocol. We then tested if GFP-positive colonies could be obtained without Sox2, Klf4, or c-Myc in the presence of M_3O with protocol B (Fig. 1D). Although M_3O still required Sox2 and Klf4, c-Myc was dispensable. Previous studies have reported that iPSCs can be established without c-Myc [18, 19]; however, the uniqueness of M_3O-SK lies in the speed and efficiency with which GFP-positive colonies form. Although it requires 3–4 weeks and the presence of feeder cells for OSK to induce GFP-positive colonies at an efficiency of around 0.01% [18, 19], M_3O-SK could generate GFP-positive colonies without feeder cells by day 7 after transduction at an efficiency of 0.44%, over 40-fold more efficient than OSK.

These striking differences between M_3O and Oct4 prompted us to evaluate the specificity of the M_3O configuration in relation to other host factors and TADs taken from other transcription factors using protocol B. First, we changed the location and number of the M_3 domain in the fusion protein with Oct4 (Fig. 1E). Second, the two TADs in Oct4 [20] were replaced with the M_3 domain in various combinations (Fig. 1F). Third, the M_3 domain was fused to Sox2 or Klf4 and tested in combination with other members of OSKM and M_3O (Fig. 1G). Although OM_3 was as effective as M_3O in iPSC creation, all other constructs were virtually ineffective. In fourth experiment, TADs taken from other powerful transactivators were fused to Oct4 (Fig. 1H), including the TADs from Tax of human T-lymphotropic virus type-1 [21], Tat of human immunodeficiency virus type-1 [22, 23], Gata4 [24, 25] and Mef2c [25]. When these TADs were fused to Oct4, none of them formed iPSC colonies. In conclusion, these TAD studies demonstrate that the M_3 domain was unique among the tested TADs in that it dramatically improved the efficiency of making GFP-positive colonies when fused to Oct4. Therefore, we focused on M_3O in the following studies.

Characterization of M_3O-iPSCs

The GFP-positive colonies that emerged on day 5 following transduction with M_3O-SKM using protocol B contained 31–143 cells in 12 colonies, with a median of 43 cells per colony. This number of cells would be produced after less than seven cell divisions assuming even division for each cell, which is strikingly small when compared with the median of 70 cell divisions needed before GFP-positive cells appear with OSKM [26]. The colonies that emerged with M_3O-SKM were usually homogenously GFP-positive from the beginning. On day 7, approximately 97% of these colonies were homogeneously GFP-positive with protocol B when compared with approximately 5% of colonies derived with OSKM obtained on day 12 with protocol A (Fig. 2A). Protocol A was used for OSKM because protocol B failed to yield a sufficient number of GFP-positive colonies. As a result, GFP-positive colonies were harvested at different time points corresponding to 2 days after the onset of GFP activation.

We further compared the quality of GFP-positive colonies obtained with M_3O-SKM and OSKM by quantitative reverse-transcription polymerase chain reaction (qRT-PCR) analysis of three pluripotency genes (endogenous *Oct4*, endogenous *Sox2*, and *Nanog*) and three fibroblast-enriched genes (*Thy1*, *Col6a2*, and *Fgf7*) [27–29]. We selected homogeneously GFP-positive colonies obtained with M_3O-SKM using protocol B and those with OSKM using protocol A to represent the best colonies for each group. Although cells were harvested at different time points corresponding to the onset of GFP activation, the interval between time points is the same. For OSKM, expression of the three pluripotency genes gradually increased during the initial week after emergence of GFP-positive colonies, indicating a slow maturation process toward pluripotency (Fig. 2B). For M_3O-SKM, in contrast, levels of these transcripts reached or exceeded those seen in ESCs at the time of the emergence of GFP-positive colonies and remained at similar levels until day 30. This differential efficiency of transcriptional reprogramming was also evident with suppression of the three fibroblast-enriched genes. For M_3O-SKM, expression levels of these genes on day 5 when the GFP signal was apparent were comparable to those seen in ESCs, but it took around 1 week after the activation of GFP for OSKM to accomplish the same level of gene suppression (Fig. 2C). Together, these results indicate that M_3O-SKM can reprogram MEFs to an iPSC state more efficiently than OSKM.

The pluripotency of iPSC clones prepared with M_3O-SKM following protocol B (M_3O-iPSCs) was verified using three standard approaches. First, genome-wide transcript analysis demonstrated highly similar gene expression in M_3O-iPSCs and ESCs. Out of 41,160 probes, 3,293 were greater than fourfold differentially expressed (upregulated or downregulated) in both ESCs and cloned iPSCs when compared with MEFs (Fig. 3A). The commonly upregulated genes included eight ESC-enriched genes, such as *Oct4*, *Sox2*, and *Nanog*. In addition, *Thy1*, *Col6a2*, and *Fgf7* were downregulated more than 16-fold in both ESCs and iPSCs. Second, intramuscular injection of M_3O-iPSCs into an nonobese diabetic/severe combined immunodeficiency (NOD/SCID) mouse resulted in teratoma formation as shown by the presence of various tissues derived from the three germ layers (Fig. 3B). Third, aggregation of eight-cell stage embryos of the ICR strain with M_3O-iPSCs containing the Oct4-GFP allele and ROSA26-*lacZ* allele formed chimeric mice (Fig. 3C, 3D). M_3O-iPSCs contributed to germ cells in some chimeric mice (Fig. 3E). When one of the chimeric males (Fig. 3D, left) was crossed with a wild-type female ICR mouse (Fig. 3F, white adult at bottom), all 11 pups showed agouti or black coat color (Fig. 3F).

Establishment of Human iPSCs with M_3O-SKM

We next evaluated if M_3O could also facilitate generation of human iPSCs in comparison with OSKM. We transduced human M_3O-SKM and OSKM into human dermal fibroblasts

prepared from a 34-year-old female. Because these cells did not harbor a transgene that could be used as a convenient marker for reprogramming, expression of the pluripotency protein NANOG was monitored by immunofluorescence staining as an iPSC indicator. NANOG-positive human ESC-like colonies emerged around day 8 with M_3O-SKM, with the number increasing by around day 15 when 0.30% ± 0.033% of the original fibroblasts were converted to iPSC colonies (Fig. 4A, 4B). In contrast, when OSKM was transduced, NANOG-positive colonies did not emerge until around day 12 and eventually only 0.0052% ± 0.0018% of the fibroblasts were turned into iPSC colonies. This indicates 58-fold increased efficiency with M_3O-SKM in comparison with OSKM. Furthermore, while less than 10% of the colonies that appeared with OSKM were NANOG positive, more than 90% of the colonies produced with M_3O-SKM were NANOG-positive, consistent with the results for mouse iPSCs. Cloned iPSCs prepared with M_3O-SKM also expressed endogenous OCT4 and surface markers stage-specific embryonic antigen 4 (SSEA4), TRA-1-60, and TRA-1-81 on day 28 (Fig. 4C). Transduced M_3O was suppressed by this day (not shown). In addition, iPSCs prepared with M_3O-SKM expressed 12 pluripotency genes as demonstrated by qRT-PCR (Fig. 4D). All the 20 mitotic spreads prepared from a cloned M_3O-SKM iPSCs demonstrated normal karyotypes (Fig. 4E). Finally, they formed teratomas when injected into an NOD/SCID mouse (Fig. 4F), proving pluripotency of the cells.

Chromatin Analyses of Pluripotency Genes in M_3O-MEFs

We used only mouse cells in all of the following experiments. To understand how M_3O-SKM facilitated nuclear reprogramming at the molecular level, we examined several chromatin changes at the *Oct4* gene during the early phase of iPSC generation. All analyses were performed with protocol B on all MEFs in a culture dish including GFP-positive and GFP-negative cells without subculture for 9 days. First, we studied changes in DNA methylation at the promoter of the *Oct4* gene. CpG dinucleotides at the proximal promoter of the *Oct4* gene are heavily methylated in MEFs, unlike in ESCs and iPSCs [30] (Fig. 5A), and this serves as a major inhibitory mechanism for *Oct4* transcription. Although the number of unmethylated CpG sites remained essentially the same on day 9 in O-MEFs, the number increased approximately twofold in M_3O-MEFs on the same day (Fig. 5A, 25.5% vs. 55.5%). The more advanced demethylation in M_3O-MEFs than in O-MEFs is consistent with the higher percentage of GFP-positive cells in M_3O-MEFs than in O-MEFs on day 9 (12.77% vs. 0.52%) as shown by flow cytometry (Fig. 5B).

Next, we studied the binding of Oct4 and Sox2 to the distal enhancer of the *Oct4* gene [31] using chromatin immunoprecipitation (ChIP). The binding of Oct4 and Sox2 to the distal enhancer remained low with O-MEFs (Fig. 5C). Importantly, however, Oct4, which was identical to M_3O in this case, was already highly bound to the *Oct4* distal enhancer in M_3O-MEFs as early as day 3 when no GFP-positive colonies had appeared yet (Fig. 5C, the red column in the Oct4 panel). The Oct4-binding level gradually increased subsequently, eventually reaching the level comparable to that seen in ESCs on day 9. The chromatin binding of Sox2 displayed a similar tendency. It was important to understand if the high binding levels of Oct4 and Sox2 on day 9 could be explained by the existing GFP-positive cells (12.77%, Fig. 5B). However, it was technically difficult to collect GFP-negative cells in the order of 1×10^7 cells with a fluorescence activated cell sorter (FACS) for ChIP analyses. As an alternative approach, we examined the binding levels of these two proteins in the mixture of ESCs and MEFs at a 13:87 ratio. This study showed substantially lower binding of Oct4 and Sox2 in comparison with the day 9 levels in M_3O-MEFs (Fig. 5C, ESCs +MEFs in blue). This observation indicates that Oct4 and Sox2 were bound to the Oct4 enhancer in the majority of M_3O-MEFs including GFP-negative cells on day 9. The increased binding of these two proteins to chromatin in M_3O-MEFs prompted us to investigate if chromatin accessibility at the distal enhancer was also increased in M_3O-

MEFs. Increased chromatin accessibility is generally indicated by higher sensitivity to DNAses [32]. We digested chromatin from M_3O-MEFs and O-MEFs with the restriction enzyme NsiI and analyzed DNA fragments using Southern blotting. Indeed, chromatin accessibility was consistently higher in M_3O-MEFs when compared with O-MEFs between days 5 and 9 (Fig. 5D). Additionally, we selected GFP-negative M_3O-MEFs with a FACS on day 9 followed by NsiI digestion analysis. This GFP-negative population also demonstrated increased sensitivity to NsiI (Fig. 5D, far right), indicating that the minor GFP-positive population did not significantly influence the overall result of chromatin accessibility.

Previous reports have shown that the Paf1 complex is recruited to the distal enhancer of the *Oct4* gene through binding to the Oct4 protein [33, 34] and then generally moves to the coding region of the gene [35]. We observed that three Paf1 complex subunits—parafibromin, Leo1, and Paf1—displayed a gradual increase of binding to the distal enhancer and coding region of the *Oct4* gene in M_3O-MEFs, but not in O-MEFs, between days 3 and 9 following transduction (Fig. 5C). The Paf1 complex recruits the histone methyltransferase complex COMPASS, which catalyzes trimethylation of lysine four on histone H3 (H3K4me3) [35]. This histone modification, a marker for active genes, was also increased specifically in M_3O-MEFs in the coding region of the *Oct4* gene (Fig. 5E). Two other markers for active genes, acetylation of lysines 9 and 14 on histone H3 (H3K9ac and H3K14ac) [36], were also increased specifically in M_3O-MEFs (Fig. 5E). In addition, two markers for suppressed genes, trimethylation of H3K9 (H3K9me3) and H3K27 (H3K27me3) [36], were more drastically decreased in M_3O-MEFs than those in O-MEFs (Fig. 5F). Similar results were observed at the *Sox2* locus (Supporting Information Fig. S2). Among these chromatin changes, the levels of H3K9me3 and H3K27me3 in M_3O-MEFs most quickly reached the levels observed in ESCs (Fig. 5F), suggesting that the loss of these suppressive histone markers precedes other chromatin modifications. Taken together, these results demonstrate that chromatin at *Oct4* and *Sox2* loci was generally remodeled in majority of M_3O-MEFs, including the GFP-negative population, toward an ESC pattern during the first 10 days after transduction, while chromatin in the majority of O-MEFs was not significantly altered.

In addition to global chromatin remodeling, M_3O-SKM also elicited wider expression of two pluripotency markers than OSKM: alkaline phosphatase and SSEA1. Alkaline phosphatase was almost ubiquitously expressed by day 9 in M_3O-MEFs, unlike the weak and heterogeneous expression observed in O-MEFs (Fig. 6A). SSEA1 was also more widely expressed in M_3O-MEFs than in O-MEFs by day 9 as shown by immunofluorescence microscopy and flow cytometory (Fig. 6B, 6C). While alkaline phosphatase and SSEA1 are not exclusively expressed in pluripotent cells, these findings support the above interpretation that M_3O-SKM remodeled the chromatin in much more wider population of the cells to a certain degree unlike OSKM. Rapid cell proliferation is known to facilitate iPSC generation as shown using p53-null MEFs [26]; however, neither M_3O-SKM nor M_3O alone facilitated MEF proliferation during the initial 9 days after transduction (Fig. 6D, 6E).

Chromatin Analyses of Pluripotency Genes Without c-Myc

M_3O-SK induced GFP-positive colonies over 100-fold more efficiently than OSKM with protocol B (0.44% with M_3O-SK in Fig. 1D vs. 0.0035% with OSKM in Fig. 1F). This observation suggests that the M_3 domain could compensate for the lack of c-Myc when *Oct4* activation was used as an indicator. Although several roles of c-Myc have been proposed, its precise function in iPSC formation remains elusive [37]. To further understand the roles of c-Myc in the activation of pluripotency genes, we repeated chromatin analyses at the *Oct4* and *Sox2* loci comparing MEFs transduced with three genes (M_3O-SK or OSK) and four genes (M_3O-SKM of OSKM) on day 9 when the effects of M_3O-SKM were readily

detectable. We also transduced one gene (M_3O or Oct4) and two genes (M_3O+Sox2 or Oct4+Sox2) for comparison. At this time point, 3.16% of MEFs were GFP-positive with M_3O-SK (Fig. 7A), and almost no GFP-positive cells were observed with other combinations of one, two, or three genes. However, M_3O-SK did not significantly decrease the overall level of DNA methylation when compared with other gene combinations (Fig. 7B).

As for transcription factor binding to the enhancer, M_3O facilitated binding of Oct4, Sox2, and parafibromin in combination with Sox2 or Sox2 and Klf4 (Fig. 7C, red), with some of these binding levels comparable to levels achieved with M_3O-SKM. However, Leo1 and Paf1 were not recruited to the enhancer without c-Myc (Fig. 7C). The binding of parafibromin, Leo1, and Paf1 to the initiation site of *Oct4* was also weak without c-Myc (Supporting Information Fig. S3A). Consistent with this partial assembly of the Paf1 complex at the *Oct4* gene, the level of H3K4me3 remained low without c-Myc (Fig. 7D; Supporting Information Fig. S3B). Another active gene maker, H3K9ac, also remained low without c-Myc (Fig. 7D; Supporting Information S3B). Whereas H3K9me3 was effectively decreased by M_3O-S and M_3O-SK, H3K27me3 was more resistant to demethylation by any of the gene combinations without c-Myc (Fig. 7E). At the *Sox2* gene, when compared with the *Oct4* gene, M_3O did not substantially increase the binding of Oct4 or Sox2 to the enhancer alone or in combination with Sox2 or Sox2 and Klf4 (Supporting Information Fig. S4A). The changes in the levels of H3K4me3, H3K9ac, H3K9me3, and H3K27me3 were all weak in the absence of c-Myc (Supporting Information Fig. S4B). Together, these chromatin studies indicate that while M_3O could facilitate formation of GFP-positive colonies without c-Myc, the overall level of chromatin remodeling in GFP-negative MEFs was low in the absence of c-Myc.

Discussion

This study advances the field of iPSC biology by showing that one of the rate-limiting steps in iPSC formation with OSKM is poor chromatin accessibility at pluripotency genes and that a strong TAD can overcome this problem. Because iPSC formation was dramatically improved with M_3O-SKM, the factors required to increase chromatin accessibility most likely already exist within MEFs but are not effectively recruited to pluripotency genes when using OSKM. Our current working model is that the MyoD TAD overcomes the barrier of closed chromatin by effectively attracting chromatin modifying proteins and thereby facilitating the binding of Oct4 and other regulatory proteins as well as epigenetic modifications at pluripotency genes (Fig. 7F). Myc family proteins have been proposed to globally relax chromatin in part through activation of the histone acetyltransferase GCN5 and in part through direct binding to thousands of genomic loci [37, 39]. Our results also support c-Myc's potential roles in chromatin remodeling although we do not know if c-Myc is located upstream of chromatin remodeling, as suggested by the direct binding of c-Myc to pluripotency genes [40], or downstream of chromatin remodeling (preferential proliferation of MEFs with remodeled chromatin).

One of the central questions related to the molecular mechanisms of iPSC formation is how closed chromatin at the loci of *Oct4*, *Sox2*, and *Nanog* are opened by OSKM. Little is known about this mechanism. One potential mechanism is that chromatin disruption occurs during repeated DNA replication as suggested by a report that 92% of B lymphocytes derived from inducible OSKM transgenic mice become iPSCs after 18 weeks of culture [26]. Additionally, knockdown of *p53* in B cells shortened both cell doubling time and the time required to form iPSCs by twofold. However, this does not seem to be the case for M_3O-SKM because it did not facilitate cell proliferation. Additionally, emerging GFP-positive colonies contained far less cells than their counterparts obtained from B cells. It has

been difficult, if not impossible, to perform biochemical analysis of the early process of iPSC formation, such as epigenetic remodeling at pluripotency genes, because of the presence of feeder cells and nonresponsive MEFs that comprise more than 90% of transduced cells. However, the MyoD TAD eliminated the requirement for feeder cells and achieved significant levels of epigenetic remodeling even in those MEFs that eventually fell short of activating GFP with protocol B. Thus, the MyoD TAD is expected to facilitate the dissection of epigenetic processes during the early phase of iPSC formation.

Wang et al. [41] recently demonstrated that the TAD of the herpes simplex virus type 1 protein VP16 facilitates iPSC generation when fused to Oct4, Sox2, and Nanog. The efficiency of making iPSCs was similar between M_3O and Oct4-VP16 when combined with Sox2 and Klf4 (0.44% with M_3O in the absence of feeder cells in Fig. 1D vs. 0.47% with Oct4-VP16 in the presence of feeder cells). However, the functions of the M_3 domain and the VP16 TAD are different in three points. First, germline-competent iPSCs can be established with Oct4-VP16 without additional factors but M_3O alone did not generate iPSCs. Second, while the M_3 domain was not effective in iPSC formation when fused to Sox2 or Klf4, the VP16 TAD was also effective when fused to Sox2 and Klf4 although the efficiency drops to approximately 0.2%. Third, whereas three tandemly repeated VP16 TADs were more powerful than a single VP16 TAD, two tandemly repeated M_3 domains were inhibitory. These differences suggest that M_3O and Oct4-VP16 promote iPSC production based on different mechanism. As for the binding proteins, many chromatin proteins are known to bind to the VP16 TAD (see [41] for references), but only p300/cAMP response element-binding (CREB)–binding protein is known to interact with the MyoD TAD [42]. Related to this, epigenetic remodeling in the MEFs transduced with Oct4-VP16 has not been characterized. The fact that these two independent studies achieved similar results of increasing iPSC production validates the power of the TAD-fusion approach in nuclear reprogramming.

By combining transcription factors with TADs, this approach to nuclear reprogramming is expected to have a range of applications from inducing pluripotency, as shown in this study, to inducing direct conversion from one differentiated cell type to another without transitioning through iPSCs [25, 43, 44]. As pointed out before, the first iPSC article initiated a new approach of identifying an essential combination of genes for nuclear reprogramming from a pool of candidate genes [1]. First, these authors simultaneously transduced all candidate genes into MEFs and, after detecting a positive effect, systematically eliminated each gene to identify a necessary and sufficient set of genes. The power of this simple and methodical approach has been repeatedly demonstrated by successful application of the same approach to identifying different sets of three sufficient genes in making pancreatic β cells, neurons, and cardiac muscle cells from other cell types by direct conversion [25, 43, 44]. However, the chance of success with this approach is constrained by an inherent limitation of the transactivation capacity of each gene product. The strategy of TAD-fusion to potentiate transactivators is expected to break this limitation and further advance the study of nuclear reprogramming. Although only the MyoD TAD was effective in our small-scale screen of TADs, the effect of each TAD is highly likely to be dependent on cell types, host transcription factors, and target genes. Other TADs have been used to amplify the activity of transcription factors. For instance, the TAD of VP16 was fused to the transcription factor Pdx1 to facilitate conversion of hepatocytes to pancreatic cells [38, 45]. However, the MyoD TAD has not been used in nuclear reprogramming. In principle, a TAD-fusion approach could be applied to combinations of many other transcription factors and TADs to amplify the activity of the host transcription factor and control cell fate decisions.

Conclusion

We demonstrated that the fusion gene between the MyoD TAD and Oct4 facilitated iPSC formation in the absence of feeder cells and c-Myc. The TAD promoted epigenetic remodeling at pluripotency genes during iPSC formation even in the cells that failed to be completely reprogrammed. Our results indicate that poor chromatin accessibility and factor recruitment is a major limiting factor of iPSC creation.

Supplementary Material

Refer to Web version on PubMed Central for supplementary material.

Acknowledgments

We thank Susan Keirstead and Michael Franklin for critical reading of the manuscript; Atsushi Asakura for the support of mouse experiments; James Dutton, Lucas Greder, Kimberly Stelzig, Kristin Voltzke, and Liying Zhang for technical support for iPSC culture; Timothy D. O'Brien for histological analyses; Wei-Shou Hu, Kartik Subramanian, and Wayne Xu for DNA microarray analyses; and Toshio Kitamura for Plat-E cells and pMXs-IP retroviral vectors. Karyotyping and histological preparation were performed at the University of Minnesota Cytogenetics Core Laboratory and the Comparative Pathology Shared Resource, respectively, in support with the comprehensive Masonic Cancer Center NIH grant (P30 CA077598-09). This work was also supported by the Richard M. Schulze Family Foundation (to M.F. and N.K.), NIH (R01 DK082430), Leukemia Research Fund, and Academic Health Center of the University of Minnesota (to N.K.).

References

1. Yamanaka S, Blau HM. Nuclear reprogramming to a pluripotent state by three approaches. Nature. 2010; 465:704–712. [PubMed: 20535199]
2. Takahashi K, Yamanaka S. Induction of pluripotent stem cells from mouse embryonic and adult fibroblast cultures by defined factors. Cell. 2006; 126:663–676. [PubMed: 16904174]
3. Huangfu D, Maehr R, Guo W, et al. Induction of pluripotent stem cells by defined factors is greatly improved by small-molecule compounds. Nat Biotechnol. 2008; 26:795–797. [PubMed: 18568017]
4. Huangfu D, Osafune K, Maehr R, et al. Induction of pluripotent stem cells from primary human fibroblasts with only Oct4 and Sox2. Nat Biotechnol. 2008; 26:1269–1275. [PubMed: 18849973]
5. Jaenisch R, Young R. Stem cells, the molecular circuitry of pluripotency and nuclear reprogramming. Cell. 2008; 132:567–582. [PubMed: 18295576]
6. Niwa H. How is pluripotency determined and maintained? Development. 2007; 134:635–646. [PubMed: 17215298]
7. Tapscott SJ. The circuitry of a master switch: Myod and the regulation of skeletal muscle gene transcription. Development. 2005; 132:2685–2695. [PubMed: 15930108]
8. Berkes CA, Tapscott SJ. MyoD and the transcriptional control of myogenesis. Semin Cell Dev Biol. 2005; 16:585–595. [PubMed: 16099183]
9. Weintraub H, Tapscott SJ, Davis RL, et al. Activation of muscle-specific genes in pigment, nerve, fat, liver, and fibroblast cell lines by forced expression of MyoD. Proc Natl Acad Sci USA. 1989; 86:5434–5438. [PubMed: 2748593]
10. Hirai H, Tani T, Kikyo N. Structure and functions of powerful transactivators: VP16, MyoD and FoxA. Int J Dev Biol. 2010; 54:1589–1596. [PubMed: 21404180]
11. Choi J, Costa ML, Mermelstein CS, et al. MyoD converts primary dermal fibroblasts, chondroblasts, smooth muscle, and retinal pigmented epithelial cells into striated mononucleated myoblasts and multi-nucleated myotubes. Proc Natl Acad Sci USA. 1990; 87:7988–7992. [PubMed: 2172969]
12. Kitamura T, Koshino Y, Shibata F, et al. Retrovirus-mediated gene transfer and expression cloning: Powerful tools in functional genomics. Exp Hematol. 2003; 31:1007–1014. [PubMed: 14585362]

13. Carey BW, Markoulaki S, Hanna J, et al. Reprogramming of murine and human somatic cells using a single polycistronic vector. Proc Natl Acad Sci USA. 2009; 106:157–162. [PubMed: 19109433]
14. Morita S, Kojima T, Kitamura T. Plat-E: An efficient and stable system for transient packaging of retroviruses. Gene Ther. 2000; 7:1063–1066. [PubMed: 10871756]
15. Lengner CJ, Camargo FD, Hochedlinger K, et al. Oct4 expression is not required for mouse somatic stem cell self-renewal. Cell Stem Cell. 2007; 1:403–415. [PubMed: 18159219]
16. Gerber AN, Klesert TR, Bergstrom DA, et al. Two domains of MyoD mediate transcriptional activation of genes in repressive chromatin: A mechanism for lineage determination in myogenesis. Genes Dev. 1997; 11:436–450. [PubMed: 9042858]
17. Weintraub H, Dwarki VJ, Verma I, et al. Muscle-specific transcriptional activation by MyoD. Genes Dev. 1991; 5:1377–1386. [PubMed: 1651276]
18. Nakagawa M, Koyanagi M, Tanabe K, et al. Generation of induced pluripotent stem cells without Myc from mouse and human fibroblasts. Nat Biotechnol. 2008; 26:101–106. [PubMed: 18059259]
19. Wernig M, Meissner A, Cassady JP, et al. c-Myc is dispensable for direct reprogramming of mouse fibroblasts. Cell Stem Cell. 2008; 2:10–12. [PubMed: 18371415]
20. Niwa H, Toyooka Y, Shimosato D, et al. Interaction between Oct3/4 and Cdx2 determines trophectoderm differentiation. Cell. 2005; 123:917–929. [PubMed: 16325584]
21. Boxus M, Twizere JC, Legros S, et al. The HTLV-1 Tax interactome. Retrovirology. 2008; 5:76. [PubMed: 18702816]
22. Romani B, Engelbrecht S, Glashoff RH. Functions of Tat: The versatile protein of human immunodeficiency virus type 1. J Gen Virol. 2010; 91:1–12. [PubMed: 19812265]
23. Pumfery A, Deng L, Maddukuri A, et al. Chromatin remodeling and modification during HIV-1 Tat-activated transcription. Curr HIV Res. 2003; 1:343–362. [PubMed: 15046258]
24. Cirillo LA, Lin FR, Cuesta I, et al. Opening of compacted chromatin by early developmental transcription factors HNF3 (FoxA) and GATA-4. Mol Cell. 2002; 9:279–289. [PubMed: 11864602]
25. Ieda M, Fu J-D, Delgado-Olguin P, et al. Direct reprogramming of fibroblasts into functional cardiomyocytes by defined factors. Cell. 2010; 142:375–386. [PubMed: 20691899]
26. Hanna J, Saha K, Pando B, et al. Direct cell reprogramming is a stochastic process amenable to acceleration. Nature. 2009; 462:595–601. [PubMed: 19898493]
27. Stadtfeld M, Maherali N, Breault DT, et al. Defining molecular cornerstones during fibroblast to iPS cell reprogramming in mouse. Cell Stem Cell. 2008; 2:230–240. [PubMed: 18371448]
28. Gonzalez F, Barragan Monasterio M, Tiscornia G, et al. Generation of mouse-induced pluripotent stem cells by transient expression of a single nonviral polycistronic vector. Proc Natl Acad Sci USA. 2009; 106:8918–8922. [PubMed: 19458047]
29. Maherali N, Sridharan R, Xie W, et al. Directly reprogrammed fibro-blasts show global epigenetic remodeling and widespread tissue contribution. Cell Stem Cell. 2007; 1:55–70. [PubMed: 18371336]
30. Okita K, Ichisaka T, Yamanaka S. Generation of germline-competent induced pluripotent stem cells. Nature. 2007; 448:313–317. [PubMed: 17554338]
31. Chew JL, Loh YH, Zhang W, et al. Reciprocal transcriptional regulation of Pou5f1 and Sox2 via the Oct4/Sox2 complex in embryonic stem cells. Mol Cell Biol. 2005; 25:6031–6046. [PubMed: 15988017]
32. Carey, MF.; Peterson, CL.; Smale, ST. In vivo analysis of an endogenous control region. In: Carey, MF.; Peterson, CL.; Smale, ST., editors. Transcriptional Regulation in Eukaryotes. New York: Cold Spring Harbor Laboratory Press; 2009. p. 261-322.
33. Ding L, Paszkowski-Rogacz M, Nitzsche A, et al. A genome-scale RNAi screen for Oct4 modulators defines a role of the Paf1 complex for embryonic stem cell identity. Cell Stem Cell. 2009; 4:403–415. [PubMed: 19345177]
34. Ponnusamy MP, Deb S, Dey P, et al. RNA polymerase II associated factor 1/PD2 maintains self-renewal by its interaction with Oct3/4 in mouse embryonic stem cells. Stem Cells. 2009; 27:3001–3011. [PubMed: 19821493]

35. Gerber M, Shilatifard A. Transcriptional elongation by RNA polymerase II and histone methylation. J Biol Chem. 2003; 278:26303–26306. [PubMed: 12764140]
36. Kouzarides T. Chromatin modifications and their function. Cell. 2007; 128:693–705. [PubMed: 17320507]
37. Knoepfler PS. Why myc? An unexpected ingredient in the stem cell cocktail. Cell Stem Cell. 2008; 2:18–21. [PubMed: 18371417]
38. Kaneto H, Nakatani Y, Miyatsuka T, et al. PDX-1/VP16 fusion protein, together with NeuroD or Ngn3, markedly induces insulin gene transcription and ameliorates glucose tolerance. Diabetes. 2005; 54:1009–1022. [PubMed: 15793239]
39. Knoepfler PS, Zhang XY, Cheng PF, et al. Myc influences global chromatin structure. EMBO J. 2006; 25:2723–2734. [PubMed: 16724113]
40. Kidder BL, Yang J, Palmer S. Stat3 and c-Myc genome-wide promoter occupancy in embryonic stem cells. PLoS One. 2008; 3:e3932. [PubMed: 19079543]
41. Wang Y, Chen J, Hu JL, et al. Reprogramming of mouse and human somatic cells by high-performance engineered factors. EMBO Rep. 2011; 12:373–378. [PubMed: 21399616]
42. Sartorelli V, Huang J, Hamamori Y, et al. Molecular mechanisms of myogenic coactivation by p300: Direct interaction with the activation domain of MyoD and with the MADS box of MEF2C. Mol Cell Biol. 1997; 17:1010–1026. [PubMed: 9001254]
43. Zhou Q, Brown J, Kanarek A, et al. In vivo reprogramming of adult pancreatic exocrine cells to beta-cells. Nature. 2008; 455:627–632. [PubMed: 18754011]
44. Vierbuchen T, Ostermeier A, Pang ZP, et al. Direct conversion of fibroblasts to functional neurons by defined factors. Nature. 2010; 463:1035–1041. [PubMed: 20107439]
45. Horb ME, Shen CN, Tosh D, et al. Experimental conversion of liver to pancreas. Curr Biol. 2003; 13:105–115. [PubMed: 12546783]

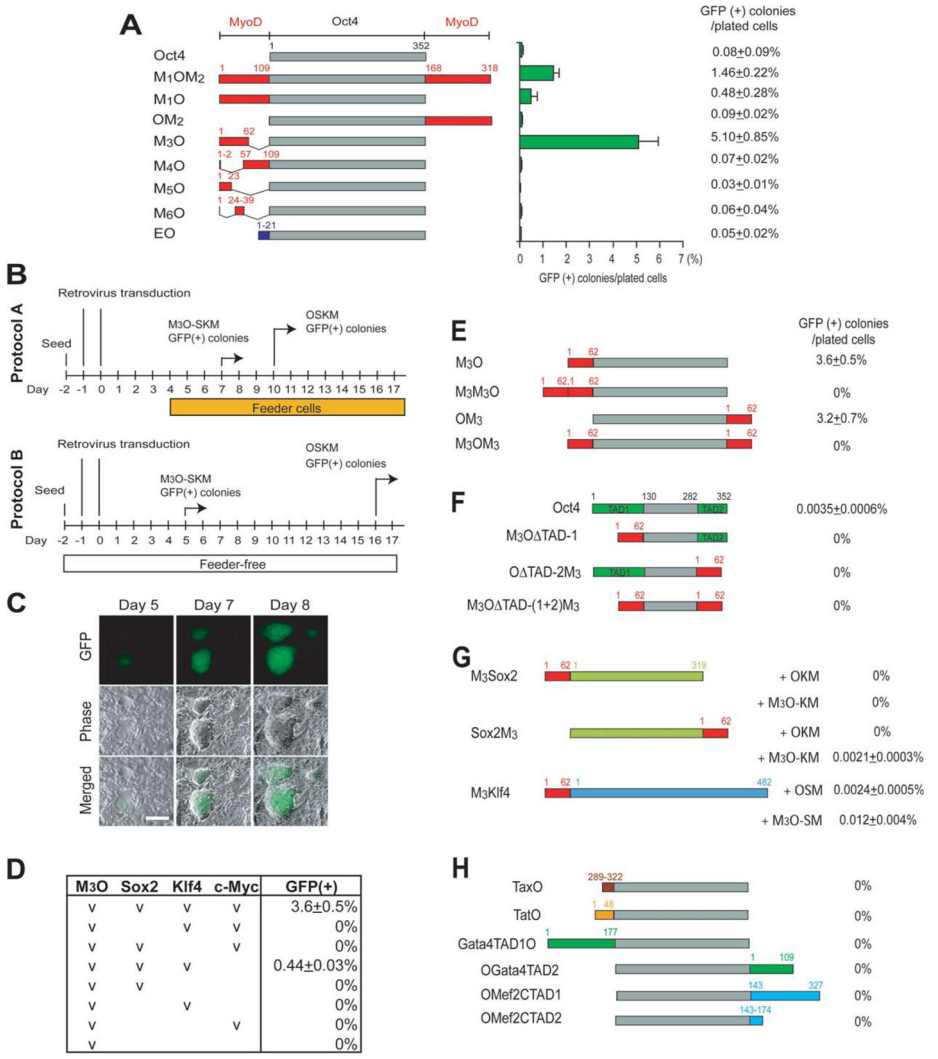

Figure 1.

Establishment of mouse induced pluripotent stem cells (iPSCs) with M_3O-*Sox2*, *Klf4*, and *c-Myc* (SKM). **(A):** Schematic drawing of MyoD-Oct4 chimeric constructs. Numbers indicate amino acid positions delimiting MyoD fragments. The basic helix-loop-helix domain of MyoD corresponds to amino acids 108–167, which was not used in these chimeric constructs. EO indicates a polypeptide consisting of one methionine and a chain of 20 glutamic acids fused to Oct4 (E for glutamic acid). Right column shows percentage of green fluorescence protein (GFP)-positive colonies derived from mouse embryonic fibroblasts (MEFs) transduced with each MyoD-Oct4 chimeric construct along with SKM and cultured on feeder cells (Fig. 1B, protocol A). Data represent the mean + SEM from three independent experiments. **(B):** Schematic drawings of two protocols for iPSC creation. Although transduced MEFs were transferred onto feeder cells on day 4 in protocol A, MEFs were maintained feeder-free until the end of experiments in protocol B. **(C):** Emergence of GFP-positive colonies obtained with M_3O-SKM with protocol B. Scale bar = 200 μm. **(D):** Summary of the efficiency of making GFP-positive colonies with various combinations of the *M_3O*, *Sox2*, *Klf4*, and *c-Myc* genes with protocol B. Number of GFP-positive colonies peaked by day 14. **(E):** Drawings of various combinations of the M_3 domain and Oct4. The efficiency of making GFP-positive colonies with protocol B in the presence of SKM is

shown on the right. **(F):** Drawings of transactivation domain (TAD) replacement constructs in which TADs of Oct4 were replaced with the M_3 domain. Constructs were transduced with SKM. **(G):** Drawings of fusion constructs between the M_3 domain and Sox2 or Klf4. Sox2 mutants were transduced with OKM or M_3O-KM. The Klf4 mutant was transduced with OSM or M_3O-SM. **(H):** Drawings of fusion constructs between Oct4 and TADs taken from other transactivators. Constructs were transduced with SKM. Abbreviations: GFP, green fluorescence protein; OSKM, *Oct4*, *Sox2*, *Klf4*, and *c-Myc*; SKM, *Sox2*, *Klf4*, and *c-Myc*.

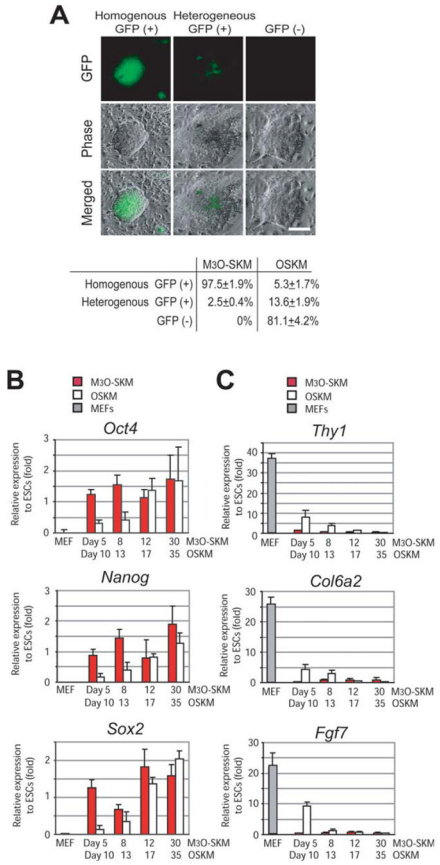

Figure 2.

Characterization of mouse M_3O-induced pluripotent stem cells. **(A):** Comparison of green fluorescence protein (GFP)-positivity between colonies obtained with M_3O-*Sox2*, *Klf4*, and *c-Myc* (SKM) and *Oct4*, *Sox2*, *Klf4*, and *c-Myc* (OSKM) using protocol B. Representative images of the GFP expression patterns used to categorize colonies are shown (top). Percentages of colonies with different GFP expression patterns were calculated from 300 colonies for M_3O-SKM and OSKM (bottom). Scale bar = 200 μm. **(B):** Quantitative reverse-transcription polymerase chain reaction (qRT-PCR) analysis of expression levels of three pluripotency genes in mouse embryonic fibroblasts (MEFs) and GFP-positive colonies obtained with M_3O-SKM and OSKM. PCR primers specific to endogenous *Oct4* and *Sox2* were used for these two genes. Although GFP-positive colonies were harvested on different days based on the time when the GFP signal first emerged for M_3O-SKM (day 5) and OSKM (day 10), the intervals between time points is equivalent (bottom of graphs). Expression level of each gene in embryonic stem cells (CGR8.8 cells) was defined as 1.0. Five colonies were examined for each condition. Results represent the mean + SEM of three independent experiments. **(C):** qRT-PCR analysis of expression levels of three fibroblast-enriched genes in MEFs and GFP-positive colonies obtained with M_3O-SKM and OSKM. Abbreviations: ESCs, embryonic stem cells; GFP, green fluorescence protein; MEFs, mouse embryonic fibroblasts; OSKM, *Oct4*, *Sox2*, *Klf4*, and *c-Myc*; SKM, *Sox2*, *Klf4*, and *c-Myc*.

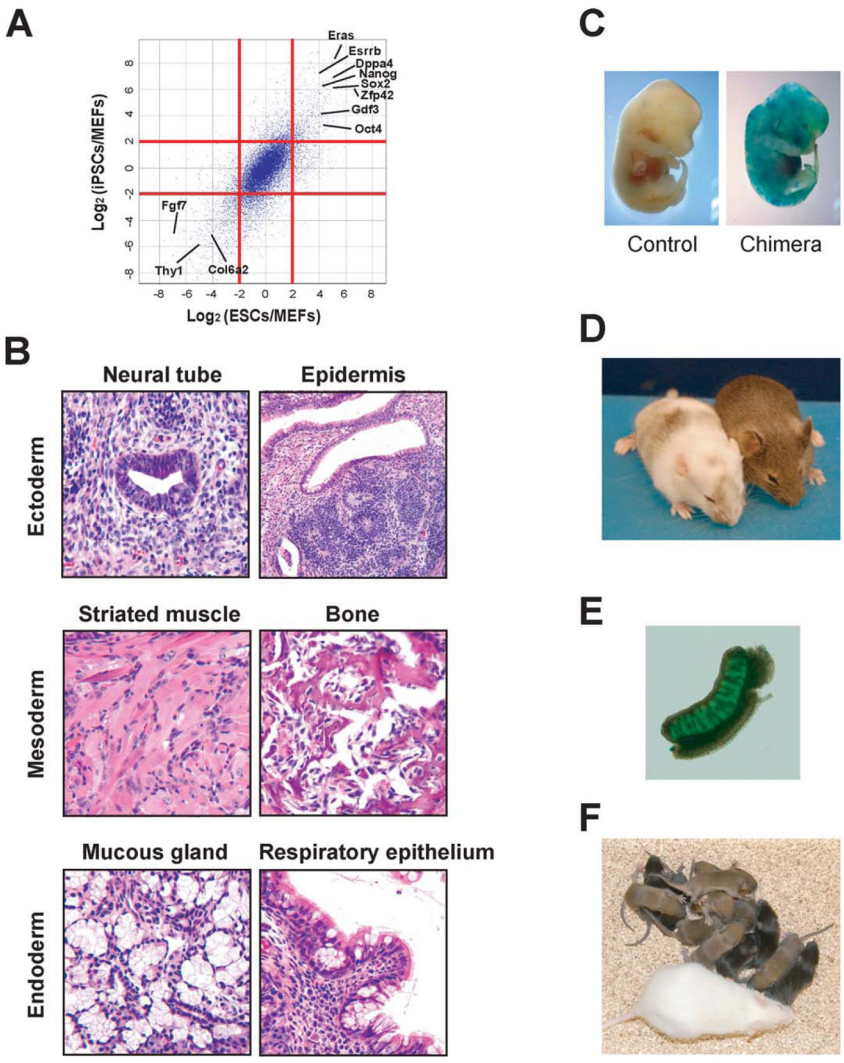

Figure 3.

Verification of pluripotency of mouse M_3O-induced pluripotent stem cells (iPSCs). **(A):** Expression level of transcripts in M_3O-iPSCs and embryonic stem cells (ESCs) relative to mouse embryonic fibroblasts (MEFs). Log2 ratios are plotted for transcripts in ESCs/MEFs and iPSCs/MEFs. Red lines indicate a fourfold difference in transcript levels. Transcripts in M_3O-iPSCs were assayed 60 days after transduction. **(B):** H&E staining of teratoma sections derived from M_3O-iPSCs. Neural tube and epidermis (ectoderm), striated muscle and bone (mesoderm), and mucous gland and respiratory epithelium (endoderm) are shown. Scale bar = 50 μm. **(C):** X-gal staining for cells expressing the *lacZ* gene in a chimeric embryo prepared with M_3O-iPSCs and a control embryo at 13.5 dpc. **(D):** Chimeric mice prepared with M_3O-iPSCs. The agouti coat color indicates a high (right) and low (left) contribution of iPSCs to the skin. The host embryos used to generate mice were derived from the albino mouse strain ICR. **(E):** Germline contribution of M_3O-iPSCs as shown by green fluorescence protein expression in the gonad of a 13.5-dpc chimeric embryo. **(F):** Pups obtained from crossing a wild-type ICR female (bottom) with an M_3O-iPSC chimeric male (left mouse in panel D). Abbreviations: ESCs, embryonic stem cells; iPSCs, induced pluripotent stem cells; MEFs, mouse embryonic fibroblasts.

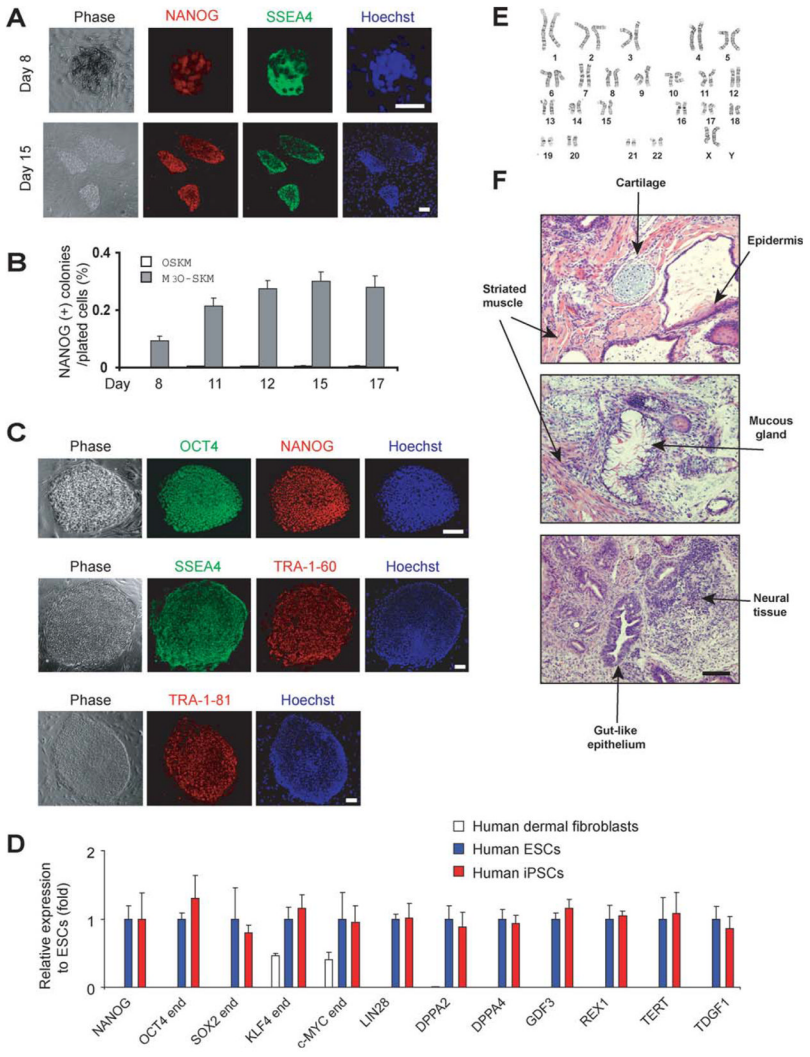

Figure 4.

Characterization of human induced pluripotent stem cells established with M_3O-*Sox2*, *Klf4*, and *c-Myc* (SKM). **(A):** Immunofluorescence staining of NANOG and SSEA4 in human iPSC colonies on days 8 and 15 obtained with M_3O-SKM without subculture after day 3 when transferred onto Matrigel. Scale bar = 100 μm for **(A)** and **(B)**. Note that day 15 colonies are substantially larger than day 8 colonies as indicated by the different magnifications. **(B):** Comparison of the efficiency of making NANOG-positive colonies between M_3O-SKM and *Oct4*, *Sox2*, *Klf4*, and *c-Myc*. The number of NANOG-positive colonies was divided by the number of seeded dermal fibroblasts at each time point. **(C):** Immunofluorescence staining of pluripotency markers in cloned human iPSCs obtained with M_3O-SKM on day 28 after four passages. **(D):** Quantitative reverse-transcription polymerase chain reaction analysis of pluripotency genes expressed in cloned human iPSCs prepared with M_3O-SKM. Ten colonies were harvested on day 30 and the mean + SEM was obtained. The expression level of each gene in human embryonic stem cells H9 was defined as 1.0. Endogenous genes were amplified for OCT4, SOX2, KLF4, and c-MYC. **(E):** Karyotype analysis of a human iPSC established with M_3O-SKM. **(F):** H&E staining of teratoma sections derived from human iPSCs prepared with M_3O-SKM. Scale bar = 100 μm. Abbreviations: ESCs, embryonic stem cells; iPSCs, induced pluripotent stem cells;

OSKM, *Oct4*, *Sox2*, *Klf4*, and *c-Myc*; SKM, *Sox2*, *Klf4*, and *c-Myc; SSEA4, stage-specific embryonic antigen 4*.

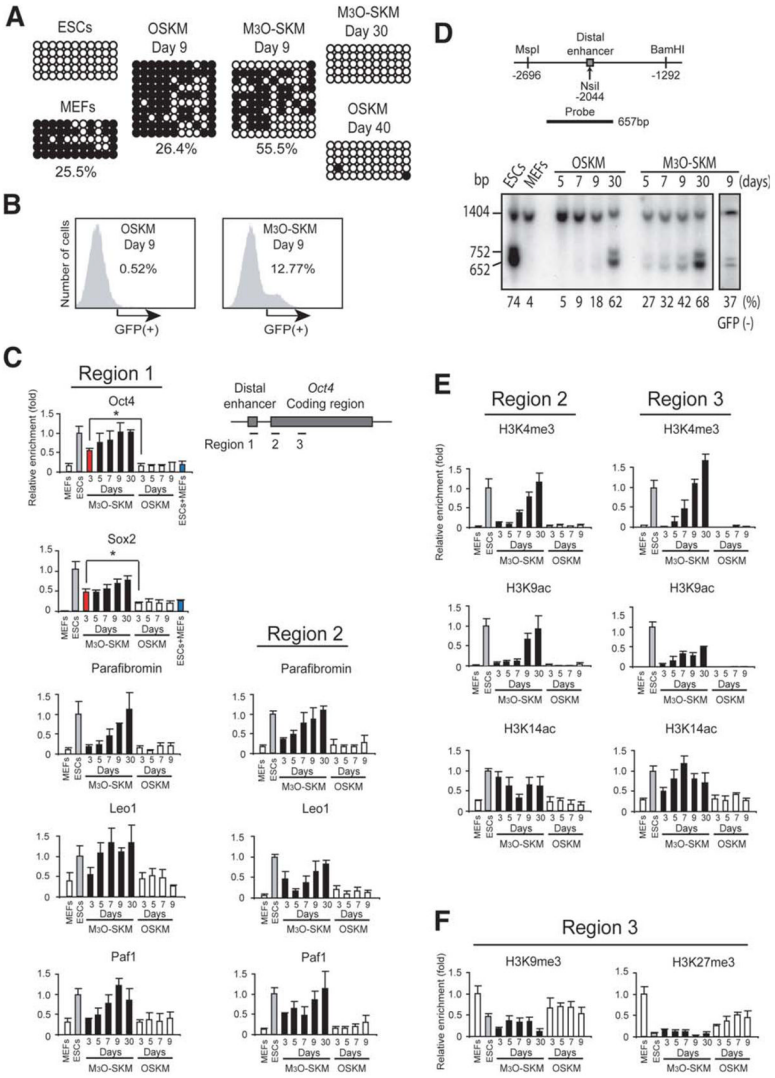

Figure 5.

Chromatin analyses of the *Oct4* gene in M_3O-mouse embryonic fibroblasts (MEFs) and MEFs with OSKM (O-MEFs). **(A):** DNA methylation patterns at the proximal promoter of the *Oct4* gene analyzed with bisulfite sequencing. Black circles indicate methylated CpG and open circles indicate unmethylated CpG. The proportion of unmethylated CpG sites was calculated by dividing the number of unmethylated CpG sites by the total number of CpG sites in each cell type. **(B):** Flow cytometry of O-MEFs and M_3O-MEFs prepared with protocol B and harvested on day 9. **(C):** Chromatin immunoprecipitation (ChIP) analyses of the binding levels of Oct4, Sox2, and Paf1 complex subunits at the distal enhancer (region 1) and initiation site (region 2) of the *Oct4* gene in M_3O-MEFs and O-MEFs. Data represent the mean + SEM of three independent experiments. All *y*-axes indicate relative enrichment (fold). Relative enrichment in embryonic stem cells (ESCs) was defined as 1.0. ESCs and MEFs were mixed at a 13:87 ratio in the sample labeled as ESCs+MEFs (blue). The difference of the values between the two samples indicated by an asterisk was statistically significant ($p < .01$). **(D):** Analyses of the accessibility of the restriction enzyme NsiI to chromatin at the distal enhancer of the *Oct4* gene by Southern blotting. Locations of the enzyme recognition site and probe are shown in relation to the distal enhancer of the *Oct4*

gene (top). The transcription initiation site was defined as position 1. Appearance of new DNA fragments following digestion with NsiI are shown (bottom). Percentage of digested chromatin was obtained by dividing the combined signal intensity of the bands at 752 and 652 bp by the combined signal intensity of the two bands and the band at 1,404 bp. Cloned O-induced pluripotent stem cell (iPSCs) and M_3O-iPSCs were used for day 30 lanes. Green fluorescence protein (GFP)-negative population was collected by a fluorescence activated cell sorter and analyzed for the day 9 GFP (−) lane of M_3O-MEFs (far right). **(E):** ChIP analyses of the levels of three histone modifications associated with active genes at the initiation site (region 2) and a coding region (region 3) of the *Oct4* gene. **(F):** ChIP analyses of the levels of two histone modifications associated with inactive genes at a coding region of the *Oct4* gene (Region 3). Relative enrichment in MEFs was defined as 1.0.
Abbreviations: ESC, embryonic stem cells; GFP, green fluorescence protein; MEFs, mouse embryonic fibroblasts; OSKM, *Oct4*, *Sox2*, *Klf4*, and *c-Myc*; SKM, *Sox2*, *Klf4*, and *c-Myc*.

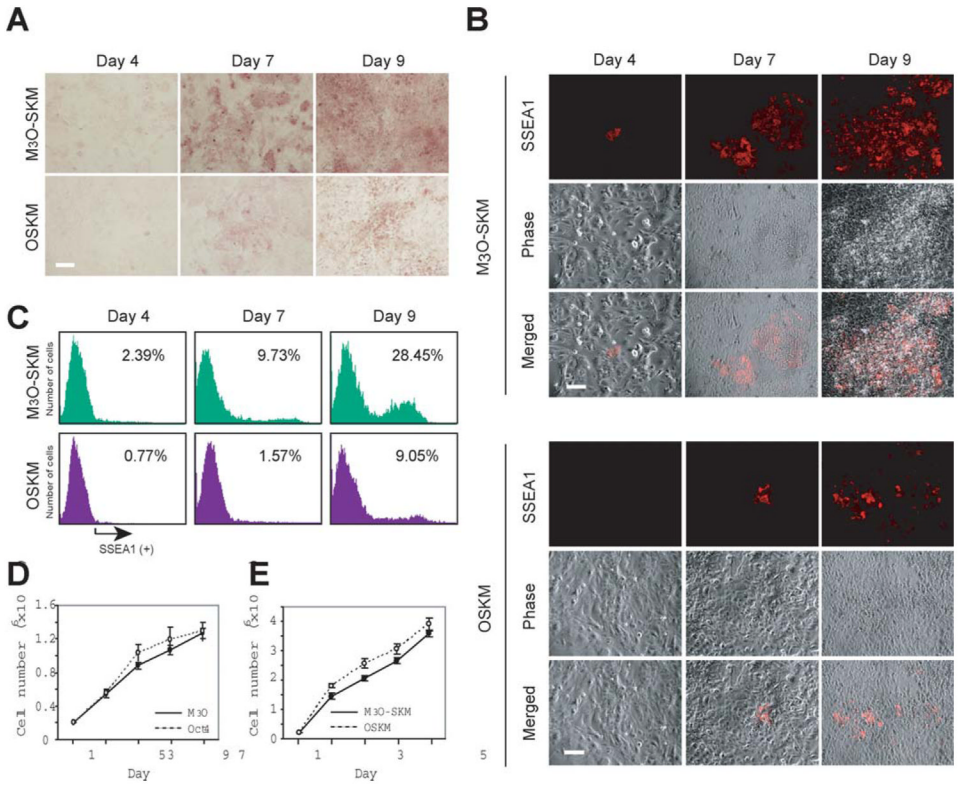

Figure 6.

Effects of M_3O-*Sox2*, *Klf4*, and *c-Myc* (SKM) and *Oct4*, *Sox2*, *Klf4*, and *c-Myc* (OSKM) on expression of pluripotency markers and cell proliferation. **(A):** Temporal profiles of expression patterns of alkaline phosphatase. Scale bar = 100 μm. **(B):** Temporal profiles of expression patterns of SSEA1. Scale bar = 100 μm. **(C):** Flow cytometry comparing the expression level of SSEA1 between mouse embryonic fibroblasts (MEFs) transduced with OSKM and those transduced with M_3O-SKM. **(D):** Cell proliferation patterns of MEFs transduced with M_3O or Oct4. Means ± SEM of three independent experiments are shown. **(E):** Cell proliferation patterns of MEFs transduced with M_3O-SKM or OSKM. Abbreviations: OSKM, *Oct4*, *Sox2*, *Klf4*, and *c-Myc*; SKM, *Sox2*, *Klf4*, and *c-Myc*; SSEA1, stage-specific embryonic antigen 1.

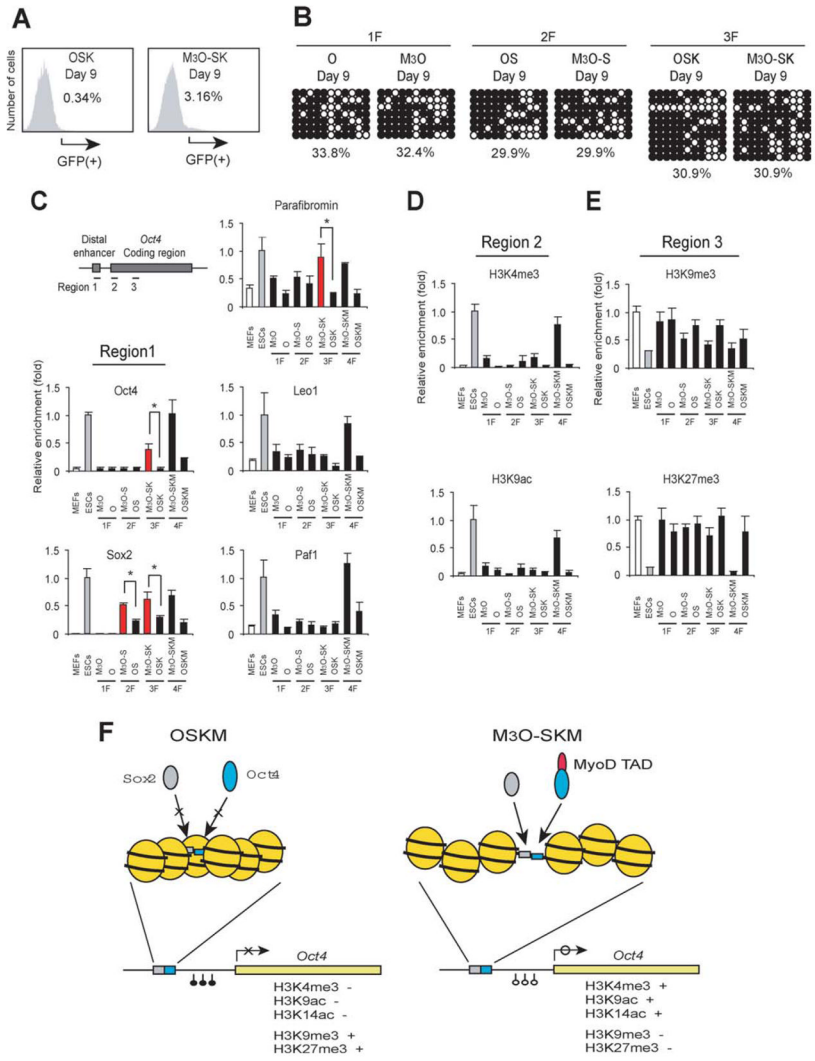

Figure 7.

Chromatin analyses of day 9 at the *Oct4* gene comparing transduction of mouse embryonic fibroblasts (MEFs) with different gene combinations. **(A):** Flow cytometry of MEFs transduced with M_3O-SK and OSK. **(B):** DNA methylation analysis by bisulfite sequencing. MEFs were transduced with one (1F), two (2F), or three (3F) transcription factor genes. **(C):** Chromatin immunoprecipitation (ChIP) studies on transcription factor binding at the distal enhancer. **(D):** ChIP analyses on histone modifications associated with active genes. **(E):** ChIP studies on histone modifications associated with suppressed genes. **(F):** Hypothetical summary of epigenetic remodeling induced by M_3O-*Sox2*, *Klf4*, and *c-Myc* (right) in comparison to the lack of remodeling with *Oct4*, *Sox2*, *Klf4*, and *c-Myc* (left). Binding sites for Oct4 and Sox2 are located adjacent to each other at the distal enhancer of *Oct4* [6]. Transduced Oct4 and Sox2 cannot bind to their respective binding sites (blue box and gray box, respectively) in the majority of MEFs with OSKM (O-MEFs) due to condensed chromatin. In contrast, M_3O and Sox2 can effectively bind to each binding site in M_3O-MEFs through the effects of the unidentified binding proteins to the MyoD transactivation domain. Recruitment of these proteins eventually contributes to DNA demethylation at the proximal promoter and a histone modification pattern typical of active genes at the coding region. Abbreviations: ESCs, embryonic stem cells; 1F, one transcription factor gene; 2F,

two transcription factor gene; 3F, three transcription factor gene; GFP, green fluorescence protein; MEFs, mouse embryonic fibroblasts; O, *Oct4*; OS, *Oct4* and *Sox2*; OSK, *Oct4*, *Sox2*, and *Klf4*; OSKM, *Oct4*, *Sox2*, *Klf4*, and *c-Myc*; S, *Sox2*; SK, *Sox2* and *Klf4*; SKM, *Sox2*, *Klf4*, and *c-Myc*; TAD, transactivation domain.